Efficient Ambiguity Resolution in Polarimetric Multi-View Stereo

A Anil Kumar, N Narendra, P Balamuralidhar and M Girish Chandra
TCS Research and Innovation, Bangalore, India.
Email:{achannaanil.kumar, n.narendra, balamurali.p, m.gchandra}@tcs.com.

***Abstract*—Polarimetric multi-view stereo (PMS) reconstructs the dense 3D surface of a *feature sparse* object by combining the photometric information from polarization with the epipolar constraints from multiple views. In this paper, we propose a new approach based on the recent advances in graph signal processing (GSP) for efficient ambiguity resolution in PMS. A smooth graph which effectively captures the relational structure of the azimuth values is constructed using the estimated phase angle. By visualizing the actual azimuth available at the reliable depth points (corresponding to the feature-rich region) as sampled graph signal, the azimuth at the remaining feature-limited region is estimated. Unlike the existing ambiguity resolution scheme in PMS which resolves only the $\pi/2$-ambiguity, the proposed approach resolves both the π and $\pi/2$-ambiguity. Simulation results are presented, which shows that in addition to resolving both the ambiguities, the proposed GSP based method performs significantly better in resolving the $\pi/2$-ambiguity than the existing approach.**

***Index terms*— Shape from Polarization, Polarimetric multi-view stereo, azimuth ambiguity, Graph signal processing**

I. Introduction

Multi-view 3D surface reconstruction is an important problem in computer vision whose application includes 3D scanning and printing, Augmented reality including products inspection [1] and many more. In many of these applications, it is most desirable to obtain dense reconstruction. However, on a *feature sparse* 3D objects, typical multi-view 3D reconstruction methods such as multi-view stereo (MVS) [1] fails to provide dense reconstruction, since it is essentially based on feature correspondence. On the other hand, the alternative photometric stereo method [2] requires active/controlled illumination for surface reconstruction. Now, when an unpolarized light is incident on a surface, most surfaces reflect a partially polarized light [3]. This polarized light contains rich information about the surface normal of the object and forms the basis for shape from polarization (SfP) cue [4]. The surface normal, thus obtained from employing this technique is dense and unlike the other above mentioned techniques, it doesn't require controlled illuminations or dense features, and hence can densely reconstruct smooth featureless 3D objects. However, the surface normals obtained from the polarization cue has certain ambiguities, which must be resolved before it can meaningfully be used for shape reconstruction.

One of the main ambiguity in using this SfP approach is in the estimation of azimuth from phase angle. Two types of ambiguities referred as π-ambiguity and $\pi/2$-ambiguity must be resolved for azimuth estimation (refer Section II for more details). While π-ambiguity arises due to the inherent estimation equation, $\pi/2$-ambiguity appears because of the unknown a priori knowledge of the nature of reflection; i.e., whether polarized specular reflection or the polarized diffuse reflection (again, Section II contains more details). Since this ambiguity being an important one to be resolved for azimuth estimation, many methods have been proposed in literature. To resolve the π-ambiguity, prior works used additional cues such as RGB-D sensor in [5] or the lighting direction [6]. Several papers simplify the $\pi/2$-ambiguity by assuming either only the polarized diffuse reflection or the polarized specular reflection such as in [4] and [7] respectively. However, in practice this is impractical [8] and as clearly demonstrated in [9], usually a mixture of both the polarized diffuse and polarized specular components shall exist. Hence, very recently, [9] proposed a new framework referred as polarimetric multi-view stereo (PMS) for dense surface reconstruction on feature sparse objects. [9] doesn't make use of the impractical assumption of polarized diffuse only or polarized specular only reflection and also overcomes the the necessity of lighting direction or the additional sensor such as RGB-D sensor. It resolves the $\pi/2$-ambiguity at feature-limited regions by using the reliable depth points at feature-rich regions which are obtained using the epipolar constraints from multiple views. [9] however doesn't resolve the π-ambiguity and bypasses it by directly estimating the depth based on the iso-contour depth tracing technique [10] using the reliable depth points as anchor points.

In this paper, we propose an alternative efficient method for ambiguity resolution in PMS framework. We effectively capture the relational structure among the azimuth values by a graph and using the recent advances in graph signal processing (GSP) the ambiguities are resolved. This relational graph itself is constructed using the estimated phase angle and by making use of the synonymity of the local absolute variation of the known phase angle field and the azimuth field; Section III contains the detailed description. By now visualizing the azimuth values (corresponding to reliable depth points) available at feature-rich region as sampled graph signal, we estimate the azimuth at feature-limited regions by using the underlying graph topology and graph signal reconstruction techniques [11]. The azimuth thus obtained, unlike in [9], shall be resolved of not only the $\pi/2$-ambiguity but also the π-ambiguity. Now with this estimated azimuth, one can use the iso-contour depth tracing method advocated in [9] for depth estimation. Alternately, the regions corresponding to the polarized specular dominant and polarized diffuse dominant regions can be classified and by employing methods described in [8], [7], the zenith angle can be estimated. Subsequently from this (azimuth, zenith) pair, depth can be estimated using a host of techniques available in the literature. Hence, with this proposed approach, the user shall have multiple choices for surface reconstruction in PMS framework. In addition, as

ISBN 978-90-827970-1-5

shall be demonstrated in Section IV through simulations that the proposed GSP based ambiguity resolution approach shows significant improvement in resolving the $\pi/2$-ambiguity than that of the label propagation approach of [9].

II. Preliminaries

In this section, we briefly present preliminaries on GSP, SfP and PMS for the sake of completeness.

A. Graph signals

Graph signals are signals whose samples are indexed by the nodes of the graph $\mathcal{G}$. $\mathcal{G} = (\mathcal{V}, \mathcal{E})$ denote a connected, undirected and weighted graph consisting of N nodes indexed by set $\mathcal{V} = \{1, 2, ..., N\}$ and connected by edges $\mathcal{E} = \{(p, q, w_{pq})\}, p, q \in \mathcal{V}$, where w_{pq} denotes the weight of the edge between p^{th} and the q^{th} node and $w_{pp} = 0$. The $N \times N$ adjacency matrix $\mathbf{W}$ with $[\mathbf{W}]_{p,q} = w_{pq}$ is a symmetric matrix (i.e., $\mathbf{W} \in \mathbb{S}^N$), due to the assumption of undirected graph [11]. The graph Laplacian is defined as $\mathbf{L} = \mathbf{D} - \mathbf{W}$, where the diagonal matrix $\mathbf{D} = \text{diag}\{d_1, d_2, ..., d_N\}$ is referred as degree matrix, and for all $1 \leq p \leq N$, $d_p = \sum_{q=1}^{N} [\mathbf{W}]_{p,q}$.

1) Graph Fourier Transform, Band-limitedness, sampling and reconstruction: In traditional discrete signal processing (DSP), the role played by the shift z^{-1} is well known; a similar role in GSP is performed by the graph shift operator $\mathbf{S}$. The typical choices for $\mathbf{S}$ usually include either the Laplacian matrix or the adjacency matrix [12], [11]. Since $\mathbf{S}$ is a symmetric matrix, it admits the factorization $\mathbf{S} = [\mathbf{u}_1, ..., \mathbf{u}_N]\text{diag}(\lambda_1, ..., \lambda_N)[\mathbf{u}_1, ..., \mathbf{u}_N]^H$. The eigenvector matrix $\mathbf{U} = [\mathbf{u}_1, ..., \mathbf{u}_N]$ and the corresponding eigenvalues $\boldsymbol{\lambda} = \{\lambda_1, ..., \lambda_N\}$ provide a notion of frequency in the context of graphs and hence the matrices $\mathbf{U}^H$ and $\mathbf{U}$ are referred as forward Graph Fourier Transform (GFT) matrix and inverse GFT matrix [11]. Now, the GFT of any graph signal $\mathbf{f}$ can be computed as $\tilde{\mathbf{f}} = \mathbf{U}^H\mathbf{f}$.

If $\tilde{\mathbf{f}}_p = \mathbf{0}$ for all p with $|\lambda_p| > \omega$ then $\mathbf{f}$ is referred as *ω-bandlimited* graph signal. Let $\mathcal{R} = \{1, 2, ..., r\}$, where r denotes the number of eigenvalues that are less than ω and $\mathbf{U}_{\mathcal{VR}}$ denote the sub-matrix of $\mathbf{U}$ containing the columns corresponding to $\mathcal{R}$. Now, the *ω-bandlimited* signal $\mathbf{f}$ can be expressed as [13]

$$\mathbf{f} = \mathbf{U}^H\tilde{\mathbf{f}} = \mathbf{U}_{\mathcal{VR}}\tilde{\mathbf{f}}. \tag{1}$$

The set $\{\mathbf{u}_1, \mathbf{u}_2, ..., \mathbf{u}_r\}$ spans a vector space which is referred as Paley-Wiener space [14] denoted by $PW_\omega(\mathcal{G})$ and essentially it consists of all ω-bandlimited signals.

The bandlimitedness allows the signal $\mathbf{f}$ to be sampled and reconstructed without any loss of information. Let $\mathcal{S}$ denote the sampling set i.e., it contains the indexes of the sampling nodes[1], with $|\mathcal{S}| = d$. Let $\mathbf{S}_d$ be a matrix of size $N \times d$ whose columns are indicator functions for $\mathcal{S}$ and the sampling operator $\mathbf{S}_d^T : \mathbb{R}^N \to \mathbb{R}^d$ [13]. The sampled vector $\mathbf{f}_\mathcal{S} = \mathbf{S}_d^T\mathbf{f}$. Correspondingly, reconstruction from the sampled signal $\mathbf{f}_\mathcal{S}$ can be achieved as [15], [13]

$$\hat{\mathbf{f}} = (\mathbf{U}_{\mathcal{VR}}(\mathbf{U}_{\mathcal{SR}}^H\mathbf{U}_{\mathcal{SR}})^{-1}\mathbf{U}_{\mathcal{SR}}^H)\mathbf{f}_\mathcal{S} \tag{2}$$

[1]Interested readers may refer to [13] and the references there-in for a detailed description of selection of the sampling set $\mathcal{S}$.

where the sub-matrix $\mathbf{U}_{\mathcal{SR}} = \mathbf{S}_d^T\mathbf{U}_{\mathcal{VR}}$. From the dimension of the matrices $\mathbf{U}_{\mathcal{SR}}$ and $\mathbf{U}_{\mathcal{VR}}$, it can easily be noticed that $d \geq r$ is a basic requirement for reconstruction.

B. Shape from Polarization

When an unpolarized light strikes a material surface, on most surfaces, the reflected light comprises of the following three components: 1) polarized specular reflection, 2) polarized diffuse reflection, and 3) the unpolarized diffuse reflection [16]. The intensity of such reflected polarized components varies sinusoidally as a function of the polarizing angle of the polarizing filter say ϕ_{pol}. In particular, the measured intensity corresponding to the polarized diffused reflection $I^{dp}(\phi_{pol})$ and the polarized specular reflection $I^{sp}(\phi_{pol})$ at a point can be expressed as [5], [6]

$$I^{xp}(\phi_{pol}) = \frac{I_{max} + I_{min}}{2} + \frac{I_{max} - I_{min}}{2}\cos(2(\phi_{pol} - \phi)) \tag{3}$$

where $x \in \{s, d\}$, and I_{max}, I_{min} denotes the maximum and the minimum values of the observed sinusoidally varying intensities respectively. The *phase angle* ϕ and the *azimuth angle* φ at any point on the surface depends upon the dominant reflection type and are related as [9]

$$\phi = \begin{cases} \varphi, \text{ if polarized diffuse reflection dominates} \\ \varphi - \frac{\pi}{2}, \text{ otherwise.} \end{cases} \tag{4}$$

The factor $I_{un} = \frac{I_{max}+I_{min}}{2}$ denotes the unpolarized intensity and the factor $\rho = \frac{I_{max}-I_{min}}{I_{max}+I_{min}}$, is referred as degree of polarization (DOP) [8]. Now, depending upon the type of the reflection i.e., either polarized diffuse or polarized specular, the DOP ρ is also related as [8]

$$\rho = \frac{2\sin\theta\tan\theta\sqrt{n^2 - \sin^2\theta}}{n^2 - 2\sin^2\theta + \tan^2\theta} \tag{5}$$

$$\rho = \frac{(n - \frac{1}{n})^2\sin^2\theta}{2 + 2n^2 - (n + \frac{1}{n})^2\sin^2\theta + 4\cos\theta\sqrt{n^2 - \sin^2\theta}} \tag{6}$$

where n and θ denotes the *refractive index* and the *zenith angle* respectively. While (5) provides the relationship for the polarized specular reflection, (6) provides the relationship for a polarized diffuse reflection. The following section describes the parameter estimation, in particular azimuth estimation[2] from the above equations and the associated ambiguities.

1) Azimuth estimation and ambiguities: By taking intensity measurements corresponding to atleast three different known polarization angles, the unknown triple $\{I_{max}, I_{min}, \phi\}$ at every pixel can be estimated by solving (3). However, the following two ambiguities; π-ambiguity and $\pi/2$-ambiguity [9], [8] in the estimated phase ϕ must be resolved for azimuth estimation. While the π-ambiguity appears due to the factor 2 present in the cosine term of (3) (notice that both $\phi = \varphi$ and $\phi = \varphi + \pi$ results in the same solution), the absence of the knowledge of the reflection type (i.e., either polarized diffuse or polarized specular (see (4))) would give rise to

[2]In this paper, we focus on azimuthal ambiguity resolution. Readers may refer to [8] for refractive index ambiguity and its resolution from multi-view images.

ISBN 978-90-827970-1-5 © EURASIP 2018

$\pi/2$-ambiguity. As mentioned in Section I, prior works use additional cues for π-ambiguity resolution and simplify the $\pi/2$-ambiguity by assuming either only the polarized diffuse or the polarized specular reflection. PMS [9], on the contrary, doesn't make these impractical assumptions and also avoids the necessity of additional sensor. The following section briefly describes the PMS.

2) Polarimetric Stereo: PMS, essentially aims to reconstruct the dense 3D surface on feature sparse objects. Further as mentioned above, [9] uses a practical setting of mixed reflection scenario (i.e., the observed polarization intensity $I = I^{dp} + I^{sp}$) and in particular showed that "no matter what the relative proportions of the polarized specular and polarized diffused reflection is, there will only be π and $\pi/2$-ambiguity in azimuth estimation". The idea of PMS setup is to capture multiple polarization images from multiple views (see [9, Figure 4]) and using the MVS method [1], a rough initial 3D shape is obtained. Since MVS methods makes use of the feature correspondence for shape estimation, the rough 3D estimated shape shall be reliable at only feature-rich regions. Now, for the other feature-limited regions, it uses the polarization images by resolving only the $\pi/2$-ambiguity with the help of the initial 3D shape. However, [9] bypasses resolving the π-ambiguity and directly estimates the depth based on the iso-contour depth tracing technique [10] with the reliable depth available at feature-rich regions as anchor points.

In the following section, by considering the azimuth at feature-rich regions as sampled signal on a graph constructed using estimated phase, we describe a new method for both π and $\pi/2$-azimuth ambiguity resolution.

III. Proposed method

A. Modified Polarimetric multi-view stereo

Fig. 1 shows the proposed *modified PMS* algorithm pipeline. Similar to [9], multiple polarized images at known different polarizing angles are captured from multiple view points of the object. Again similar to [9] by employing the standard MVS algorithm [1], initial approximate 3D shape is obtained. Since it is well known that these techniques are based on feature correspondence, this step shall provide a reasonably good estimate at the feature-rich regions. To reconstruct the shape at other feature-limited regions we make use of the polarization images. From the captured polarization images, the triple $\{I_{max}, I_{min}, \phi\}$ at every point and at every view is estimated by solving (3). Now, as shall be described in the next section, the azimuth φ is estimated from the phase angle ϕ by resolving both the π and $\pi/2$ ambiguities using the initial 3D shape. By comparing the ϕ and φ, the polarized specular reflection dominant and the polarized diffuse reflection dominant regions can easily be classified. Based on this classification, using prior works such as [8], zenith θ (using (5) or (6)) can be obtained as indicated in Fig. 1. Using the pair (φ, θ), one can now easily estimate the depth by standard surface integration or alternately use only φ with the iso-contour depth tracing approach suggested in [9].

B. Resolving the π and $\pi/2$ ambiguity

The idea is to estimate the azimuth values at feature-limited region by using the known azimuth values at feature-rich region by exploiting the relational structure among the azimuth values. The rest of this section describes the proposed approach for building the graph to effectively capture the relationship and to use it for azimuth estimation.

1) Graph Construction: It is important to note the following two observations:
i) With only the polarized diffuse or the polarized specular reflection, the *absolute* change of the phase angular field and azimuth field is *synonymous* i.e., the absolute angular distance among the respective phase angle values and azimuth values in a small neighborhood region is similar.
ii) However, the change in the reflection type on the object causes abrupt change in the phase angular field by $\pi/2$.
Now by using the estimated phase angle values and by utilizing the above observations, we build a graph which effectively captures the relational structure among the azimuth values.

Let $N_x \times N_y$ be the captured polarization image size and $N = N_x N_y$ denote the number of pixels in the image. An N node graph indexed by the set $\mathcal{V} = \{1, 2, ..., N\}$ is first constructed. Now, for any p, $(1 \leq p \leq N)$, ϕ_p denotes the phase angle at node p and further, between any two nodes $(p, q) \in \mathcal{V}, p \neq q$, the edge weight w_{pq} is computed as

$$w_{pq} = \begin{cases} g(\phi_p, \phi_q), \text{ if } g(\phi_p, \phi_q) < \epsilon_g \text{ and } \text{dist}(p, q) < \epsilon_d \\ 0, \text{ otherwise} \end{cases} \tag{7}$$

where the function $g(\phi_p, \phi_q) = \min(|\phi_i - \phi_j + \pi/2|, |\phi_i - \phi_j - \pi/2|, |\phi_i - \phi_j|)$ and $\text{dist}(p, q)$ denotes the Euclidean distance between the position of the pixels p and q. $g(\phi_p, \phi_q)$ computes the distance between the two angles ϕ_p and ϕ_q and it can easily be noticed that it is invariant to the change in the phase angle $\pi/2$ due to change in reflection type. The factors ϵ_g and ϵ_d decides the neighborhood region. Now, using these edge weights, the remaining attributes of the graph such as the graph Laplacian $\mathbf{L}$, the GFT matrix $\mathbf{U}$ are estimated as described in Section II-A. The following section describes the method for obtaining the azimuth using these graph attributes.

2) Estimation of azimuth: Now, let $\boldsymbol{\phi}, \boldsymbol{\varphi} \in \mathbb{R}^N$ denote a vector of phase angles and azimuth respectively which can be expressed as $\boldsymbol{\phi} = [\phi_1, \phi_2, ..., \phi_N]^T$ and $\boldsymbol{\varphi} = [\varphi_1, \varphi_2, ..., \varphi_N]^T$, where for any p, $(1 \leq p \leq N)$ similar to ϕ_p, φ_p denotes the azimuth at node p. Knowing $\boldsymbol{\phi}$, the graph and azimuth at feature-rich region, the problem now is to estimate $\boldsymbol{\varphi}$,

The GFT of $\boldsymbol{\phi}$ and $\boldsymbol{\varphi}$ can be computed as $\tilde{\boldsymbol{\phi}} = \mathbf{U}\boldsymbol{\phi}$ and $\tilde{\boldsymbol{\varphi}} = \mathbf{U}\boldsymbol{\varphi}$. Recalling that $\boldsymbol{\phi}$ is nothing but the ambiguous estimate of $\boldsymbol{\varphi}$, it is easy to notice that with the graph edge constructed using (7), both $\tilde{\boldsymbol{\phi}}$ and $\tilde{\boldsymbol{\varphi}}$ have similar smoothness[3], i.e., both have same cut-off frequency ω or in other words $\tilde{\boldsymbol{\phi}}, \tilde{\boldsymbol{\varphi}} \in PW_\omega(\mathcal{G})$. Let $\mathcal{V}^+$ denote the set of vertexes corresponding to feature-rich regions for which a reliable depth information, thereby unambiguous azimuth is available. The

[3]smoothness assumption on graph signals is formalized in terms of bandlimitedness, for more details interested readers may refer to [13].

ISBN 978-90-827970-1-5

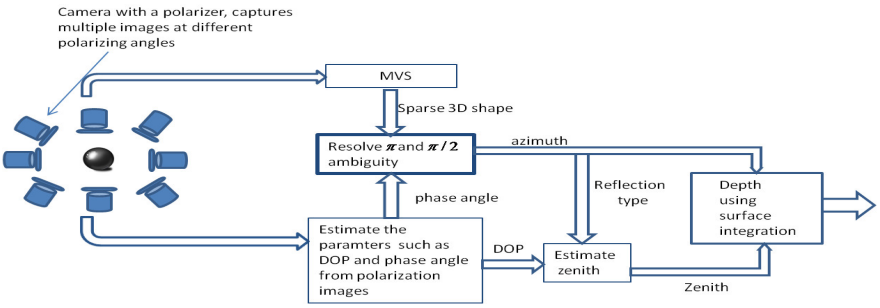

Fig. 1: Flow chart of the proposed modified polarimetric multi-view stereo algorithm pipeline. With this proposed approach the user can either obtain the depth directly from azimuth using the approach of [9] or get the surface normal.

graph signal $\boldsymbol{\phi}_{\mathcal{V}^+} \subset \boldsymbol{\phi}$, $\boldsymbol{\varphi}_{\mathcal{V}^+} \subset \boldsymbol{\varphi}$ denotes the phase angles and the azimuth respectively corresponding to graph indexes $\mathcal{V}^+$. Since the phase angle corresponding to the set $\mathcal{V}^+$ is unambiguous, $\boldsymbol{\varphi}_{\mathcal{V}^+} = \boldsymbol{\phi}_{\mathcal{V}^+}$. Now, it is important to observe that the set $\mathcal{V}^+$ and signal $\boldsymbol{\varphi}_{\mathcal{V}^+}$ is analogous to the sampling set $\mathcal{S}$ and the sampled graph signal $\mathbf{f}_{\mathcal{S}}$ (see Section II-A). From this analogy and the sampled azimuth $\boldsymbol{\varphi}_{\mathcal{V}^+}$, using (2), the azimuth signal $\boldsymbol{\varphi}$ can be estimated as

$$\boldsymbol{\varphi} = (\mathbf{U}_{\mathcal{V}\mathcal{R}}(\mathbf{U}_{\mathcal{V}^+\mathcal{R}}^H\mathbf{U}_{\mathcal{V}^+\mathcal{R}})^{-1}\mathbf{U}_{\mathcal{V}^+\mathcal{R}}^H)\boldsymbol{\varphi}_{\mathcal{V}^+} \tag{8}$$

where $\mathbf{U}_{\mathcal{V}^+\mathcal{R}}$ is similar to $\mathbf{U}_{\mathcal{S}\mathcal{R}}$ and the set $\mathcal{R}$ can be found by observing the GFT spectrum $\tilde{\boldsymbol{\phi}}$, since $\tilde{\boldsymbol{\phi}}, \tilde{\boldsymbol{\varphi}} \in PW_\omega(\mathcal{G})$ as mentioned above. In practice, it is important to note that the cut-off ω is determined by putting a threshold on the spectrum of $\tilde{\boldsymbol{\phi}}$, since spectrum doesn't exactly go to zero. The estimated $\boldsymbol{\varphi}$ using the above equation will be resolved of not only the $\pi/2$-ambiguity but also the π-ambiguity. As mentioned in Section II-A, $|\mathcal{V}^+| > |\mathcal{R}|$ is a basic requirement for obtaining appropriate $\boldsymbol{\varphi}$.

C. Comparisons with [9]

The following are the important differences between the proposed approach and the method of [9]:
i) Unlike [9] which solves only for the $\pi/2$-ambiguity, the proposed approach solves for both the π and $\pi/2$-ambiguities. ii) [9] solves the $\pi/2$-ambiguity by formulating it as a binary labeling problem and uses belief propagation for propagation of labels. Statistical priors (refer [9, Section 4.2]) which are performance sensitive are required for this algorithm. On the contrary, the proposed approach uses GSP framework and overcomes the necessity of these performance sensitive priors. iii) Since, the proposed approach solves for both the ambiguities, the user now can use either the iso-contour depth tracing approach of [9] for depth estimation or other alternative approaches of estimating the zenith θ. Subsequently, using the pair (φ, θ) at every point on the surface, depth can be estimated with many techniques available in literature.

IV. Simulation Results

In this section, we present the simulation results on the synthetic bunny. While we observed similar results on other test objects, due to lack of space we provide results only on synthetic bunny. Both the azimuth angles and zenith angles are calculated from the ground truth shape, and using (3) five polarized images corresponding to five different polarization angles $\{0, 30, 60, 90, 120\}$ are obtained. Now, the phase angle $\boldsymbol{\phi}$ is estimated at every point by solving (3). Fig. 3(a) and Fig. 3(b) shows the actual ground truth azimuth and the estimated phase angle respectively. From these figures the ambiguity can easily be noticed.

Using these estimated phase angles, the graph, as described in Section III-B1, is constructed by assuming $\epsilon_d = 10$ and $\epsilon_g = \pi/6$. Corresponding GFT matrix is also obtained and Fig. 2 shows the magnitude plots of the GFT of the actual azimuth and the estimated phase angle, with respect to the graph frequencies $\boldsymbol{\lambda}$. Notice from the figure that both have similar lowpass like bandlimitedness, thus demonstrating the well captured relational structure of azimuth values using estimated phase values. Hence, using $\tilde{\boldsymbol{\phi}}$ we decide the cut-off graph frequency. Observe from figure that after a graph frequency of 50, the magnitude becomes negligible and hence we fix the cut-off frequency of $\omega = 50$ and the corresponding $|\mathcal{R}| = 70$.

Now, we choose the size of the sampling set i.e., $|\mathcal{V}^+|$ to be 100 (around 13%) and the indexes of the sampling location set $\mathcal{V}^+$ are randomly chosen. At these locations we assume that the actual azimuth is known, and by using (8) the azimuth corresponding to other locations are estimated. The Fig. 3(a) shows the estimated azimuth, from which it can be observed that it is in close agreement with the ground truth azimuth shown in Fig. 3(b).

Next, we compare the performance of the proposed approach with that of [9] for classification of polarized specular dominant and polarized diffuse dominant reflection regions. For this simulation, we generated the polarized diffuse dominant and polarized specular dominant regions in a checker pattern as shown in Fig. 4(a). While the regions corresponding to the white shows polarized specular dominant, the regions shown in black shows polarized diffuse dominant. We choose 70 samples (around 9% of the samples) for the unambiguous locations and Fig. 4(b) and Fig. 4(c) shows the classification results obtained with the proposed approach and with that of [9] respectively. From the figure, it is clearly evident that for the same given number of samples, the proposed approach provides better classification than that of the [9]. During the simulations, it was observed that the performance of [9] is sensitive to the statistical priors required for the specular and diffuse regions. Hence, the performance of the proposed approach was compared with that of [9] for different statistical priors. Fig. 5 shows the misclassification percentage with

ISBN 978-90-827970-1-5 © EURASIP 2018

different a priori probabilities and with increasing number of unambiguous azimuth samples. From the figure, it can be noticed that with increase in *a priori* probability, the performance of [9] improves (which is along the expected lines), but despite a relatively high *a priori* probability of 0.7, the proposed GSP based approach clearly outperforms the label propagation approach of [9].

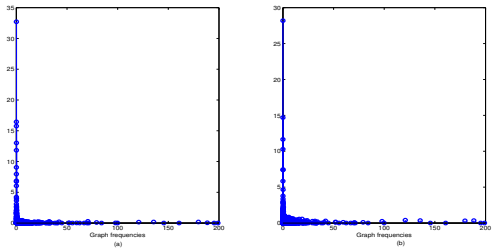

Fig. 2: Figure shows the magnitude spectrum vs graph frequencies. (a) $|\tilde{\phi}|$ vs $\boldsymbol{\lambda}$, (b) $|\tilde{\varphi}|$ vs $\boldsymbol{\lambda}$. Notice the similar bandlimitedness from both the plots.

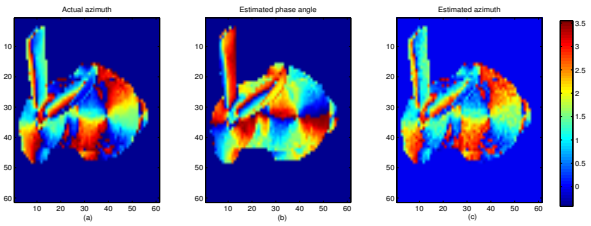

Fig. 3: Azimuth field of the synthetic bunny. (a) shows the actual ground truth, (b) shows the estimated phase angle field and (c) shows the estimated azimuth with the proposed approach after ambiguity resolution.

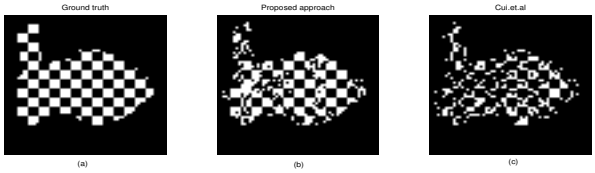

Fig. 4: Region corresponding to the white box and black box shows the polarized specular dominant and polarized diffuse dominant regions respectively on a synthetic bunny. (a) shows the ground truth, (b) shows the classification obtained with the proposed approach and (c) shows the classification obtained with cui.et.al [9].

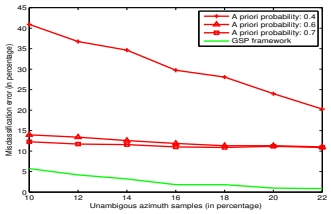

Fig. 5: Plot shows the misclassification error vs the number of unambiguous azimuth samples of the approach of [9] for different statistical priors and the proposed GSP framework based approach.

V. Conclusion

A graph, which reveals the relational structure between the azimuth values is constructed using the estimated phase angle values by exploiting the relationship between the azimuth and the phase angle. Treating available azimuth values at reliable depth points (in PMS like setup) as the sampled graph signal, this paper presented a new approach based on GSP for ambiguity resolution in azimuth estimation. The graph Fourier spectrum of the estimated phase angle revealed the important information such as the cut-off frequency and the minimum requisite samples (in the feature-rich regions) for unique estimation of azimuth (in feature-limited regions). The proposed technique resolved both the pi and $pi/2$-ambiguities and further performed significantly better than the existing state-of-art approach of [9] for $pi/2$-ambiguity resolution. The outputs of this technique can be further leveraged for dense depth reconstruction of feature sparse objects in PMS by invoking any of the standard existing procedures.

References

[1] Y. Furukawa, C. Hernández *et al.*, "Multi-view stereo: A tutorial," *Foundations and Trends® in Computer Graphics and Vision*, vol. 9, no. 1-2, pp. 1–148, 2015.

[2] R. J. Woodham, "Photometric method for determining surface orientation from multiple images," *Optical engineering*, vol. 19, no. 1, p. 191139, 1980.

[3] L. B. Wolff and T. E. Boult, "Constraining object features using a polarization reflectance model," *IEEE Transactions on Pattern Analysis and Machine Intelligence*, vol. 13, no. 7, pp. 635–657, 1991.

[4] G. A. Atkinson and E. R. Hancock, "Recovery of surface orientation from diffuse polarization," *IEEE transactions on image processing*, vol. 15, no. 6, pp. 1653–1664, 2006.

[5] A. Kadambi, V. Taamazyan, B. Shi, and R. Raskar, "Polarized 3d: High-quality depth sensing with polarization cues," in *Proceedings of the IEEE International Conference on Computer Vision*, 2015, pp. 3370–3378.

[6] W. A. Smith, R. Ramamoorthi, and S. Tozza, "Linear depth estimation from an uncalibrated, monocular polarisation image," in *European Conference on Computer Vision*. Springer, 2016, pp. 109–125.

[7] D. Miyazaki, T. Shigetomi, M. Baba, R. Furukawa, S. Hiura, and N. Asada, "Surface normal estimation of black specular objects from multiview polarization images," *Optical Engineering*, vol. 56, no. 4, p. 041303, 2016.

[8] V. Taamazyan, A. Kadambi, and R. Raskar, "Shape from mixed polarization," *arXiv preprint arXiv:1605.02066*, 2016.

[9] Z. Cui, J. Gu, B. Shi, P. Tan, and J. Kautz, "Polarimetric multi-view stereo," in *Proceedings of the IEEE Conference on Computer Vision and Pattern Recognition*, 2017, pp. 1558–1567.

[10] Z. Zhou, Z. Wu, and P. Tan, "Multi-view photometric stereo with spatially varying isotropic materials," in *Computer Vision and Pattern Recognition (CVPR), 2013 IEEE Conference on*. IEEE, 2013, pp. 1482–1489.

[11] D. I. Shuman, S. K. Narang, P. Frossard, A. Ortega, and P. Vandergheynst, "The emerging field of signal processing on graphs: Extending high-dimensional data analysis to networks and other irregular domains," *IEEE Signal Processing Magazine*, vol. 30, no. 3, pp. 83–98, 2013.

[12] A. Sandryhaila and J. M. Moura, "Discrete signal processing on graphs," *IEEE transactions on signal processing*, vol. 61, no. 7, pp. 1644–1656, 2013.

[13] A. Anis, A. Gadde, and A. Ortega, "Efficient sampling set selection for bandlimited graph signals using graph spectral proxies," *IEEE Transactions on Signal Processing*, vol. 64, no. 14, pp. 3775–3789, 2016.

[14] I. Pesenson, "Sampling in paley-wiener spaces on combinatorial graphs," *Transactions of the American Mathematical Society*, vol. 360, no. 10, pp. 5603–5627, 2008.

[15] S. Chen, R. Varma, A. Sandryhaila, and J. Kovaevi, "Discrete signal processing on graphs: Sampling theory," *IEEE Transactions on Signal Processing*, vol. 63, no. 24, pp. 6510–6523, 2015.

[16] D. A. LeMaster and M. T. Eissmann, *Multi-dimensional imaging*. Chapter Passive Polarimetric Imaging, John Wiley & Sons, 2014.

ISBN 978-90-827970-1-5